

# Height-Gradiently-Tunable Nanostructure Arrays by Grayscale Assembly Nanofabrication for Ultra-realistic Imaging

Guangzhou Geng, Ruhao Pan,\* Chensheng Li, Ruixuan Zheng, Yunan Liu, Zhongshan Zhang, Changzhi Gu, and Junjie Li\*

Due to the limitation of nanofabrication technology, nanostructured arrays and devices are usually of equal height, and it is difficult to change simultaneously its height in the Z direction at X–Y direction regulation. However, the tunable height as an indispensable part of structural spatial freedom control is very conducive to the functional expansion and innovation of nanodevices. Here, a grayscale assembled fabrication method is developed by combining e-beam lithography with atomic layer deposition and transfer technology, and a wide range of the height gradient of nanostructures can be realized in the same array and then applied in high-quality images. Following this strategy, ultra-realistic relief-nanostructured images with 256 grayscale levels are demonstrated, consisting of height-varying nanopillars with 100 nm in pixel size and  $6.4 \times 10^{10}$  dpi in resolution. Especially, multi-dimensional structural color based on metasurfaces with C4 symmetric pixels is designed and prepared by height regulation nanofabrication, enabling a strong multi-dimensional control ability in hue, saturation, and brightness of the structural color display with the single pixel of 1.5  $\mu\text{m}$  in size. The as-developed grayscale nanoconfigurations open a new approach for multidimensionally structural regulations, showing great applied potential not only in high-resolution imaging but also in more advanced nanophotonic devices.

## 1. Introduction

Nano-configurations with multi-dimensional controllable features have attracted wide concerns in many fields, including micro/nano electro-mechanical systems,<sup>[1]</sup> optoelectronic devices,<sup>[2]</sup> and optical components.<sup>[3]</sup> Nowadays, all kinds of fabrication arts, such as lithography,<sup>[4]</sup> deposition,<sup>[5]</sup> and etching<sup>[6]</sup>

have been well developed to achieve complex nanoarchitectures for versatile nanodevices. Especially for the micro/nano-photonics devices, whose performance relies heavily on the shapes and the arrangements of the nanoscale structures in the devices,<sup>[7]</sup> and moreover, diversified nano-configurations with specific features have been demonstrated to have the ability of tuning the wavefront, polarization,<sup>[8]</sup> amplitude,<sup>[9]</sup> and the phase<sup>[10]</sup> of the electromagnetic waves, and thus to be utilized in various micro/nano-photonics fields.

Usually, the performance of micro/nano photonic devices mainly depends on structure regulation of artificial structure array in the X–Y plane, but a structure regulation of Z-axis direction (or the height) of the nanostructures is always neglected because it can hardly be independently or simultaneously varied with X–Y axis on the same array due to the limitation of nanofabrication technology. As a brand-new tunable degree of spatial freedom along Z-axis direction,

the introduction of height regulation will improve the spatial regulation ability of the nanostructures and can bring more opportunities for light field manipulation to realize more versatile photonic devices with higher performance, smaller footprint, and more novel properties, compared to the planar equal-height devices.<sup>[11]</sup> For instance, metasurfaces, which consist of subwavelength resonators, can achieve functions such as focusing,<sup>[12]</sup> hologram,<sup>[13]</sup> structured light,<sup>[14]</sup> and displays<sup>[15]</sup> by an ultrathin thickness. Some theoretical studies have been reported to confirm that the height-gradient metasurfaces possess the advantage of higher efficiency, more compact configurations compared to the 2D one,<sup>[16]</sup> because the controllable degree along the z-axis gives a wide range controllability of both phase and amplitude of the incident waves. Thus, a precisely regulation of the height for the nanostructures in the same array is very desired for multi-purposes of micro/nano-photonics devices.

To fabricate micro/nanoscale structures with tunable heights, tremendous efforts have been made and various fabricating technologies have been developed, which is typified as the 3D print method. Although 3D architectures with arbitrary shapes can

G. Geng, R. Pan, C. Li, R. Zheng, Y. Liu, Z. Zhang, C. Gu, J. Li  
Beijing National Laboratory for Condensed Matter Physics  
Institute of Physics  
Chinese Academy of Sciences  
Beijing 100190, China  
E-mail: panruhao@iphy.ac.cn; jjli@iphy.ac.cn

J. Li  
Songshan Lake Materials Laboratory  
Dongguan, Guangdong 523808, China

 The ORCID identification number(s) for the author(s) of this article can be found under <https://doi.org/10.1002/lpor.202300073>

DOI: 10.1002/lpor.202300073

be built up by 3D print, this method in fact has a limited critical size and cannot be used in nanofabrication so far.<sup>[17]</sup> Notable, the two-photon absorption method, which can be treated as a 3D print method on sub-micrometer scale, has been established to fabricate polymer structures with considerable spatial controllability.<sup>[18]</sup> However, the practical application of the fabricated nanostructures is still challenged due to the limited materials and the slow processing speed of the method while its feature size is still > 100 nm. There are other approaches such as focused ion beam (FIB) induced deposition,<sup>[19]</sup> UV lithography,<sup>[20]</sup> etc. have been proved to have the ability to construct structures with controllable height. However, the FIB cannot fabricate nanostructures over a large scale due to the one-by-one fabrication mode, while the UV lithography does not have the ability of nanofabrication, namely the operating time and the nanoscale features can still hardly be achieved simultaneously. Besides, there is an interesting means that can achieve height-varying nanostructures by the clogging effect of nanoapertures during the metal deposition,<sup>[21]</sup> which is a convenient method, but the spatial controllability of the fabricated structures is still limited for the height of the nanostructure related to their linewidth. Among all the nanofabrication means, electron beam lithography (EBL) is widely applied in pattern generator for the nanoscale precision and shape controllability, and grayscale lithography of EBL carries new opportunities of fabricating height varying structures in nanoscale. Some reports have demonstrated that the EBL grayscale lithography can fabricate height-varying nanostructures, such as some nanosteps<sup>[22]</sup> or nanogratings,<sup>[18b]</sup> and nanoholes,<sup>[23]</sup> but the fabricated structures are mostly based on the resist without versatile 3D configurations and abundant alternative materials, not to mention expending it to a more general fabrication method. Consequently, the grayscale EBL should be further optimized and improved to achieve nano-configurations with diversified materials and multi-dimensional regulated features, including the height and X–Y direction structure parameter. We have demonstrated a series of high aspect ratio nanostructures, such as nanopillar, nanotube, and nanowall, based on the atomic layer deposition (ALD) by filling of nanopatterned template obtained by EBL,<sup>[24]</sup> which verified the powerful processing ability of ALD. If the EBL grayscale lithography and the ALD assembly method can be further combined, it is hoped that multi-dimensional nanostructures with selective materials, various shapes, and especially individually tuned height can be realized.

In this work, we developed a grayscale assembled nanofabrication (GANF) method based on EBL and ALD together with transfer-process, by which high aspect ratio nano-architectures with tunable height can be fabricated over a large area. The grayscale lithography of EBL is first adopted to write resist nanoholes with different depths on a sacrificial layer, and then ALD was introduced to fill the nanoholes, followed by transferring the nanostructures to the target substrate by removing the sacrificial layer, the nanostructures with different heights can finally be obtained after removing the residual resist. The height and the shapes of the nano-configurations can be precisely controlled by the EBL dose, and the nanostructures with linewidth down to 50 nm and the aspect ratio of up to 10:1 can be built up. Thanks to the GANF method, a new design for micro-image devices with both grayscale and structural color display ability

have been proposed and achieved by height regulation. As for the grayscale images, a dose correction process is utilized, and nanopillar arrays with heights linear to the gray levels of the original image are realized and results in a microscale imaging ability with 256 grayscale levels, the pixel size of 100 nm and ultra-high-resolution of  $6.4 \times 10^{10}$  dpi. In addition, the structural color is further displayed by the metasurface consisting of independent tuned heights, periods, and widths of the nanopillars. With the high spatial controllable degrees of the metasurface, it achieves the complete control of color hue, saturation, and brightness (HSB) at a high-resolution of  $2.8 \times 10^8$  dpi (1.5  $\mu\text{m}$  for each pixel), showing consistent color with the original pictures. The introduction of varied heights into structure spatial freedom degree by the GANF realizes truly the multi-dimensional structural regulation, which gives a brand-new possibility to ultra-high-resolution display components, but also constructs a powerful 3D nanofabrication platform for the design and realization of on-chip micro-displays systems, cryptography and more optical metasurface devices.

## 2. Results and Discussion

The GANF method is illustrated in **Figure 1a**, including EBL grayscale nanopattern, ALD assembly filling, patterns transfer and etching treatment process. The fabrication of the height-varying nanostructures starts from the spin-coating of the sacrificial layer, which is chosen as a kind of water-soluble film on a planar substrate. After that, e-beam resist with 800 nm in thickness is coated onto the sacrificial layer. EBL is further employed to write the designed nanopatterns with various electron irradiation dose, and resist nanoholes with changed depths are developed as a grayscale template. Then, ALD is applied to fill the nanoholes with  $\text{TiO}_2$ , which has a large index and low loss. Here, the ALD was chosen for its excellent sidewall coating property, precise thickness controllability, and the ability of depositing materials with outstanding optical parameters. The PMMA/ $\text{TiO}_2$  bilayer is peeled off from the substrate following by the sacrificial layer dissolving, and the bilayer can be rolled over and placed on the target substrate such as quartz or silicon. Finally, the  $\text{TiO}_2$  nanostructures with different heights are successfully built up after removing the resist and the underneath  $\text{TiO}_2$  film by reaction ions etching process. In order to control the structure heights at will, a contrast curve, which is the dependence between e-beam dose and residual resist, has been established in **Figure 1b**, where the high voltage is set to 100 KV, and the residual resist refers to the thickness ratio of resist after and before development. A 100  $\mu\text{m}$  square is chosen as the test pattern and the thickness of the residual resist is measured at the center point of the square. It can be clearly seen that the thickness of the resist (PMMA 950K) decreases slowly when the e-beam dose is < 400  $\mu\text{C cm}^{-2}$ , while if the dose is larger than 400  $\mu\text{C cm}^{-2}$ , the thickness decreases dramatically to 0 for a dose of 530  $\mu\text{C cm}^{-2}$ . However, when it comes to nanoscale pattern with 200 nm in width, as **Figure 1c** and **Figure S1** (Supporting Information) show, the needed e-beam dose for the same residual resist thickness becomes much larger compared to the large area pattern due to the decrease of the back-scattering electrons. Another point is, with the nanopillars' height changes from 70 to 800 nm, the width of

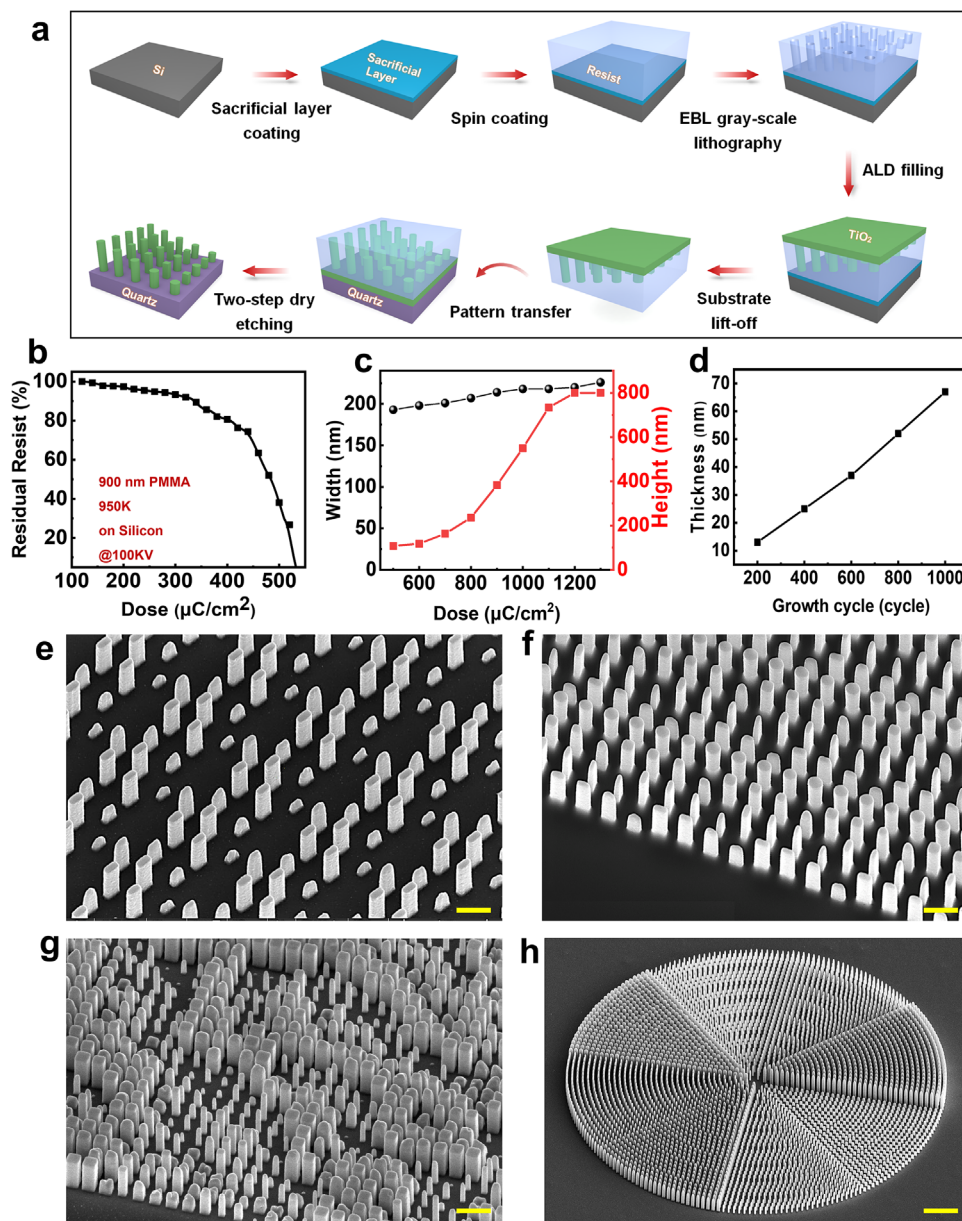


**Figure 1.** The GANF method and typical  $\text{TiO}_2$  nanostructures array with varying heights. a) A schematic of the grayscale assembly method for height varying nano-configuration based on grayscale EBL, ALD, and transfer process; b) Contrast curve of the PMMA 950K for e-beam with 100 KeV energy; c) Height and width of 200 nm nanopillar as a function of the exposure dose; d) The thickness of  $\text{TiO}_2$  film changes with the ALD cycles; Typical SEM images of  $\text{TiO}_2$  nanopillars with randomly varying height e), periodically changing height with different shapes and arrangements f), and simultaneous change in three dimensions of nanopillars along with X–Y–Z directions g, h) Circular arranged nanostructures with height gradient variation. Scale bar: (e, f) 500 nm; (g) 1  $\mu\text{m}$ ; and (h) 2  $\mu\text{m}$ .

the pillars only increases 30 nm, which means that the line width of the nanostructure shows a weak dependency on the e-beam dose. Furthermore, the precise thickness controllability of ALD is perfectly embodied in the GANF method (Figure 1d), and thus hollow or solid nanopillars with different heights and side wall thicknesses can be controlled and fabricated according to our designs.

Following the above, a series of typical nano-architectures with varying heights are built up. Figure 1e f shows a nanopillar array with randomly varied heights and with periodically changed

heights as well as various shapes, respectively. Especially, Figure 1g demonstrates a simultaneous structural change in three dimensions of nanopillars along with X–Y–Z directions, showing a large degree of spatial control freedom. Figure 1h shows a circular arranged nanopillar array, the nanopillars in the array have the largest aspect ratio up to 10:1, indicating the GANF method has the ability of fabricating high aspect ratio nano configurations. Thus, as-developed GANF method shows great controllability in the realization of 3D regulated nanopillars with arbitrary controlled height, shape, and arrangement.

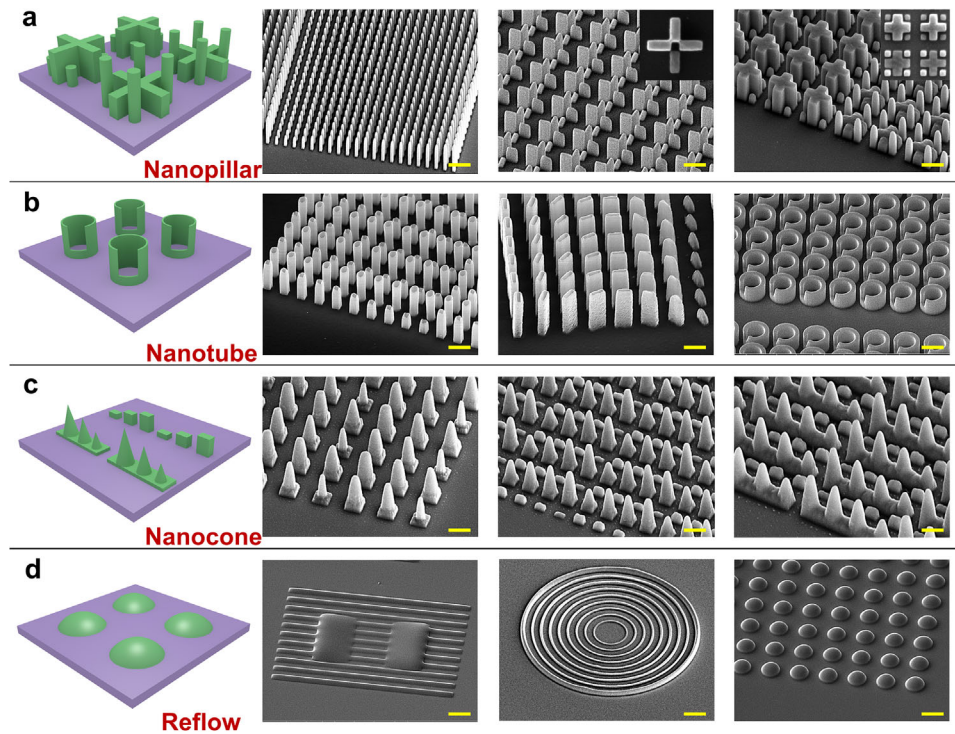


**Figure 2.** The nanofabrication ability of GANF method and its structural regulatory diversity shown by using schematic (left) and SEM images (right). a) Height varying nanopillars and the combination structure of varied-height nanopillars and cross structure; b) Nanotubes with different heights and shapes; c) Nanocones with different heights and changing radius; d) Structures by the reflow process for a smoother surface, from the left to the right are a combination of smooth nanograting and nanoslope, nanorings, and nanospheres. Scale bar: (a,c,d) 1  $\mu\text{m}$ ; (b) 500 nm.

To further explore 3D nano-construct ability of GANF method, some more special complex and combined shape nanostructures with heights regulation are fabricated successfully by using  $\text{TiO}_2$ . **Figure 2a** shows a nanopillar array with regular varied heights, whose diameter is fixed at 80 nm, but the height changes from 100 to 800 nm, indicating a highest aspect ratio of 10:1. And two other nanostructures including a nanocross array of unit cell with different heights (arms' length: 300 nm, height: 100/500/700/800 nm) and a combination of nanopillars and nanocross (heights: 800 nm or 250 nm) are also depicted, respectively. Indicating that the height can be flexibly modulated between and within different nanostructures. And the nanotubes with different heights can also be built up by tuning the ALD deposition cycles, and particularly some nanotubes with special shapes are also constructed, as shown in **Figure 2b**, where the sidewall thicknesses from left to right are 60, 80, and 100 nm, respectively. **Figure 2c** further shows a series of nanocones with bottom radius ranged from 100 to 400 nm, whose radius are changing with the height, showing extreme shape controllability of the GANF method at nanoscale. It should be noted that the dielectric structures sometimes possess a rough surface, which inherits from the roughness of the resist after development, which is often generated by machine-induced tiny dose variations during exposure or developer solution minimal shaking. A 135  $^\circ\text{C}$  reflow process is introduced to get a smooth surface,<sup>[25]</sup> which is based on heating the resist over the glass transition temperature and the rough surface is reflowed to a smooth one, where a series of  $\text{TiO}_2$  structures with smooth surface including nanograt-

ing, nanorings, and nanospheres are obtained and shown in **Figure 2d**. The nanogratings in **Figure 2d** have a period of 2  $\mu\text{m}$ , and the linewidth is fixed at 1  $\mu\text{m}$ , the concentric annulus shown in the middle image demonstrate distinctive height (from 75 to 600 nm) for each ring, and the width of the rings is 200 nm, and the nanospheres in the last image have a radius of 1  $\mu\text{m}$ . The as-developed GANF method shows superior shape controllability of the nanostructures based on large range height regulation, diversified nanoarchitectures with desirable configurations can be fabricated. The outstanding fabrication capacity of the GANF method paves the way for the design and the realization of a wide range of high-performance functional devices.

From the above, we can see that continuously adjusting the height by the GANF method will add a new controllable degree of freedom to the nanostructures and nanodevices to improve its properties and functions, which is demonstrated by taking below the high-resolution images of both grayscale and structural color as an example.

**Figure 3** shows the process of height regulation in a grayscale image painting by the GANF method. Compared to the grayscale patterns based on nanostructures with fixed height,<sup>[26]</sup> where the grayscale of the image can only be composed of binary gray levels or a single pixel containing a large number of structures. Although there are works using Malus's law to achieve images with continuously tuned gray levels by the rotation of the equal-height structures,<sup>[27]</sup> polarizers and analyzers are essential during the observation. It is difficult for equal-height configurations to construct grayscale images with enough gray orders and can

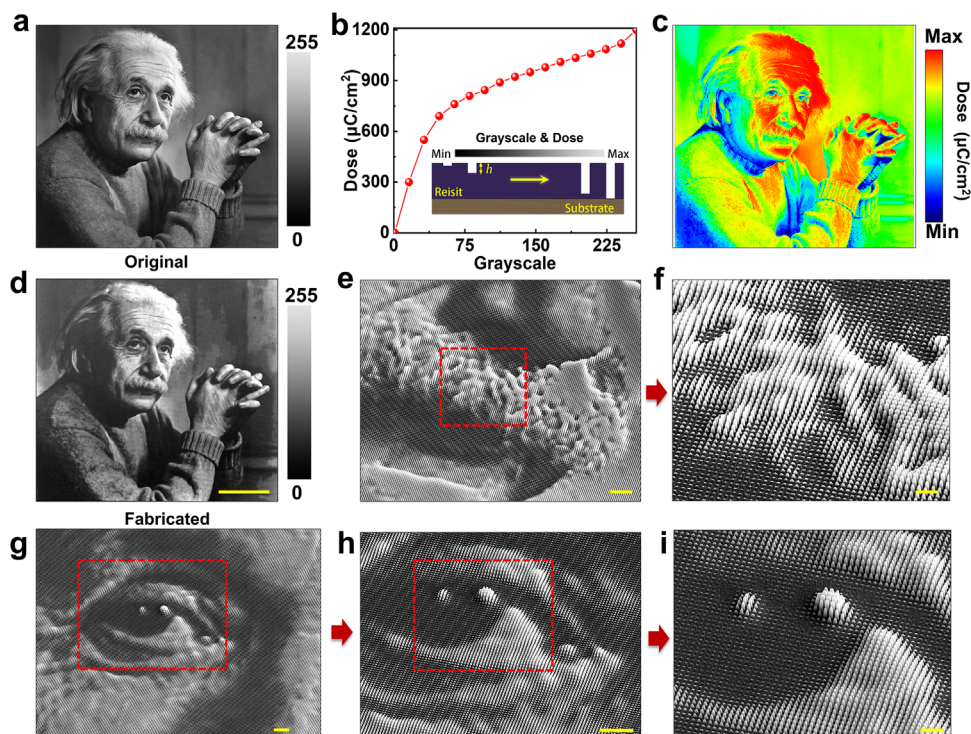


**Figure 3.** The establishment of height-regulated grayscale images by GANF. a) Original grayscale photograph of the famous scientist Einstein; b) Target dose versus the grayscale of original image, and an inset schematic shows that height grayscale at different doses can be adjusted from 0 to 255 levels in principle; c) The outputted dose mapping for the fabrication of grayscale patterns; d) Height-regulated grayscale image based on (a) with ultra-realistic grayscale imaging ability; e, f) Step by step enlarged SEM images of the beard area with full details of height regulation; g–i) Step by step enlarged SEM images of the eye area with ultra-high-resolution. Scale bar: (d) 30  $\mu\text{m}$ ; (e, g, h) 3  $\mu\text{m}$ ; (f, i) 1  $\mu\text{m}$ . The photograph of Einstein was taken by Yousuf Karsh and is used courtesy of the Albert Einstein Archives, the Hebrew University of Jerusalem, with permission from representatives of Yousuf Karsh.

be directly observed, while height gradient nanostructures may achieve this goal. Figure 3a shows an original grayscale photograph of famous scientist Einstein, which has a grayscale up to 256 levels. To build up nanoscale structures with height linear to the grayscale of the original images, a one-to-one corresponding relationship between the e-beam dose to the gray level is established, which can serve as a model of dose correction for any grayscale patterns, as shown in Figure 3b. Following this nonlinear relationship between the dose and the grayscale, with the dose increasing from 0 to 1200  $\mu\text{C cm}^{-2}$ , the depths of the developed nanoholes show a linear increasing trend, leading to a grayscale that is consistent with the original picture after the pattern transferred to height varying nanostructure. The inset of Figure 3b further demonstrates the 256 controllable levels of height can be obtained by varying the dose. Hence, a corresponding dose map can be obtained, as shown in Figure 3c, where the red area refers to the pattern with higher grayscale, while the blue area refers to the lower one. Compared to the dose map without dose correction (Figure S2, Supporting Information), the dose distribution can be clearly distinguished, which can ensure a good grayscale consistency between the original picture and the height-varying pattern. Based on the layout, a height-varying nanopillar array is constructed to present a microscale image with ultrahigh resolution, as shown in Figure 3d, which has an almost consistent gray level with the original photo and very realistic imaging effect. The edge length of the grayscale picture is 150  $\mu\text{m}$ , where the

nanopillars with 150 nm in width are arranged in an array with a period of 300 nm, and the maximal height of the nanopillar is 800 nm. Among them, the beard and the eyes are the two most distinctive parts in this grayscale photography, both which can be completely ultra-realistic displayed by our method. Figure 3e, f further demonstrates an enlarged view of the beard area of the fabricated grayscale structures, from which we can clearly see some local details that the heights of the nanopillar are changed dramatically, leading to the grayscale changes of the image. Thanks to the advancement of the GANF method, the heights of the nanopillars are independent from each other even for the pixel size of 300 nm. In addition, Figure 3g–i further demonstrates the step-by-step enlarged images of the eye area, in which the clear fluctuation of the nanopillars array really reflects the change of height and meets the requirements of high-resolution imaging, confirming fully outstanding grayscale controllability of the developed GANF method.

Following the above strategy of grayscale imaging by GANF, structure parameters of grayscale image, such as the image size, pixel size, and resolution, can be further tuned and optimized to verify the ultra-high-resolution display ability of the GANF method. In Figure 4a, a famous grayscale image of "Girl with A Pearl Earring" (painted by Johannes Vermeer) is regulated, where the edge width of this image is fixed at 40  $\mu\text{m}$  while the pixel size is shrunk from 400 to 100 nm. It can be clearly seen that the image becomes much smoother and more exquisite

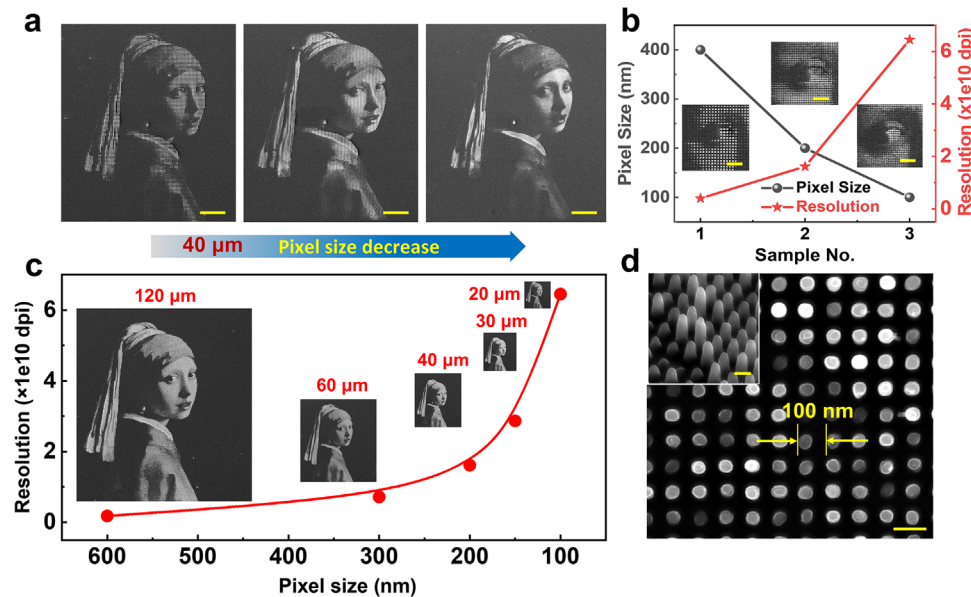


**Figure 4.** Ultra-high-resolution display ability of the grayscale imaging in microscale by height-tunable nanopillar. a) Along the arrow, the pixel sizes are decreased but pixel numbers are increased for height tunable grayscale patterns at a fixed edge length (40  $\mu\text{m}$ ); b) The pixel size and resolution of grayscale images in (a), the insets of the eye area indicate that the fabricated patterns become finer with the pixel size decrease; c) Image resolution versus pixel size, where grayscale patterns have the same pixel number but changed pixel sizes, results in the edge length of the grayscale pattern shrunk from 120 to 20  $\mu\text{m}$ ; d) A top view of nanopillar array with 100 nm period, and an inset depicts a tilted SEM image that clearly shows nanopillars with different heights and gray levels. Scale bar: (a) 5  $\mu\text{m}$ ; (b) 2  $\mu\text{m}$ , and (d) 100 nm. Image) J. Vermeer, Girl with a Pearl Earring, 1665, Mauritshuis, The Hague.

with the decrease of the pixel size. Figure 4b summarizes the pixel size and the resolution of the fabricated structures in Figure 4a, and the resolution increased dramatically with the pixel size decrease to reach the maximum of  $6.4 \times 10^{10}$  dpi. The insets of Figure 4b are enlarged views of the eye area, compared to the grayscale images with 400 nm in pixel size, the pixel with 100 nm period can barely be distinguished and have more superior display performance. Figure 4c shows the dependence of pixel size on the resolution, and the inset further shows the corresponding grayscale images with fixed pixel numbers but changed picture sizes from 120 to 20  $\mu\text{m}$ . Notably, the edge length of the image could even reach down to 20  $\mu\text{m}$  for pixel size of 100 nm, indicating that the developed method has the ability for the fabrication of microscale images. Figure 4d is the detailed view of the nanopillars of the images with 20  $\mu\text{m}$  in edge length, showing that nanoscale pixel with size down to 100 nm can be reliably fabricated. And the inset demonstrates the tilted view of the pixels with 100 nm size, indicating that the height controllability is still effective for the structure with 100 nm period, 50 nm diameter, and a resolution of  $6.4 \times 10^{10}$  dpi. Compared to the grayscale images constructed by planer patterns with pixel size  $> 100$  nm and limited gray levels, the GANF method for height-varying nanostructures gives a fresh possibility to microscale grayscale pictures with abundant grayscale and ultra-high resolution. Especially the 256 grayscale pixels in nanoscale can hardly be achieved by the conventional method that only has spatial controllability along x and y directions, indicating the GANF method can be potentially used as copy-right markers and anti-counterfeit features in microchips.<sup>[26]</sup> Notably, although the grayscale images demonstrated in Figures 3 and 4 are captured

by a SEM, they still show grayscale that consistent with the SEM under the illuminating of white-light as Figure S3 (Supporting Information) shows, indicating a wide range of application scenarios.

In addition of ultra-high-resolution grayscale images, tunable height of nanostructures can also be adopted to the design of structural color metasurface with advanced functions. The structural color that comes from the interaction of light and the optical structures shows distinct advantages including high-resolution, stability in extreme environments (e.g., acidic/alkaline or high temperatures environments) compared to the chemical dyes. Nowadays, structural color not only demonstrates great application potentials in high-resolution displays, but also in camouflage<sup>[28]</sup> and encryption devices.<sup>[29]</sup> However, the traditional processing method can only achieve structures with limited spatial controllability, resulting in that the color HSB cannot be individually regulated by the metasurface. Recently, there are works have achieved the multi-dimensional control of the HSB by introducing the rotation of the unit cells<sup>[30]</sup> demonstrating that an additional controllable degree of the structures can improve the color control range, but the large pixel sizes and the polarization-sensitive properties limited the resolution and the observation of the images. Fortunately, GANF method gives a new possibility to construct structural color images with high resolution, multi-dimensional controlled color, and polarization-insensitive properties. In this work, we introduce a height dimension to the traditional structural color, designing and constructing a height-varying metasurface, which is composed of arranged pixels with area of  $1.5 \mu\text{m} \times 1.5 \mu\text{m}$  on a 100 nm/150 nm thick  $\text{TiO}_2/\text{Al}$  layer, each pixel refers to an array of nanopillars that

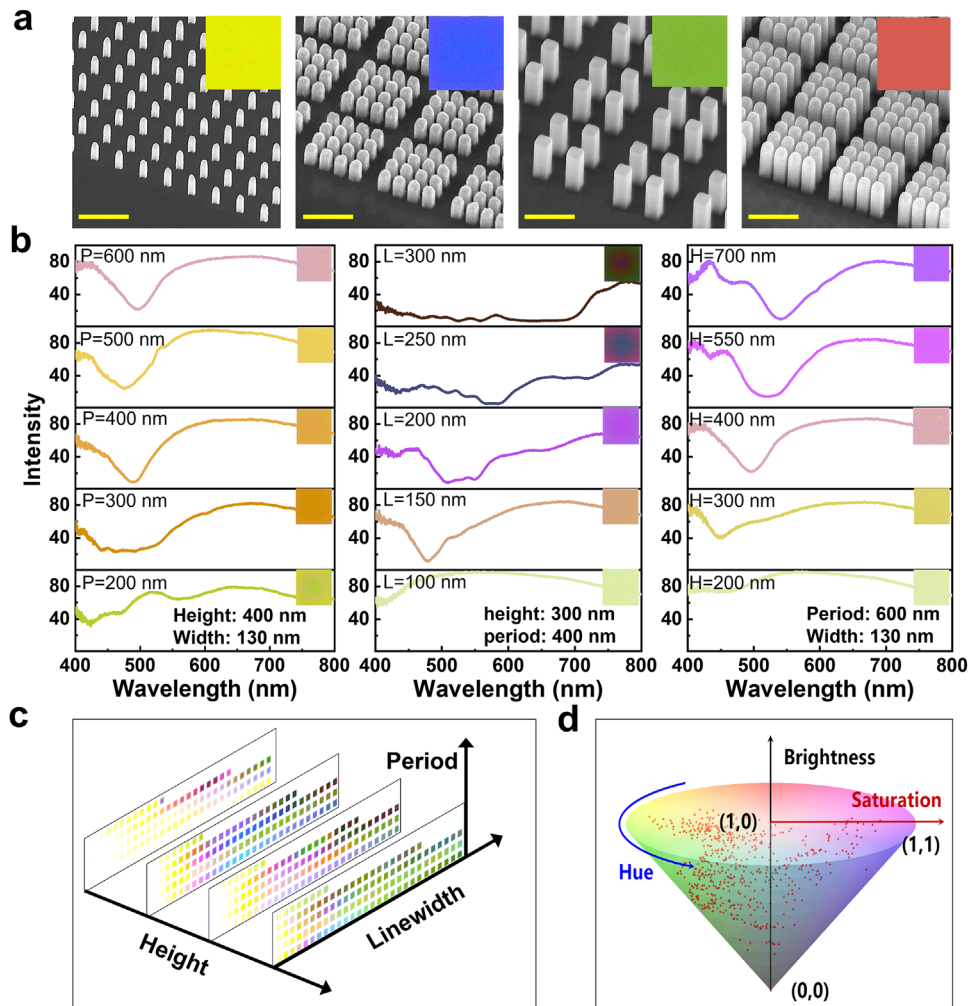


**Figure 5.** Pixelated structural color obtained by height varying metasurface consisted of square-shaped nanopillar. a) SEM images of the structural color metasurface with different configurations in three dimensions including heights, and the insets show the collected colors; b) From left to right are reflection spectra of the pixel arrays with changed periods, edge widths and heights, respectively, while the other parameters are fixed; c) 3D color map based on the length, period, and height of the unit cell in the pixels; d) Distribution of structural colors collected from metasurfaces with different feature sizes in HSB color space. Scale bar: 1  $\mu\text{m}$ .

displays a specific color. As shown in **Figure 5a**, the pixels are composed of a square nanopillar array with C4 symmetry, indicating the structural color does not rely on the incidence polarization. Here, we use the array of pixels rather than the large-area periodic nanopillar array to determine the displayed color. Because when the structural color metasurface used in image display, the distance of the nanopillar is inevitably inhomogeneous, the utilization of pixel array can guarantee the accuracy of the results for the distance inhomogeneity of the nanopillars from different pixels are considered. And the displayed color of the corresponding metasurface is further shown in the inset, different colors such as yellow, blue, green, and red can be observed uniformly and vibrantly. To better understand the color display ability of the height-varying metasurface, a series of pixel arrays with different widths (80–300 nm), periods (200–600 nm), and heights (200–700 nm) has been built up by the GANF method. **Figure 5b** gives the collected reflection spectra of the pixel arrays, in which the left panel shows the spectra of pixels with a height of 400 nm

and a length of 130 nm, while the periods of the unit cells in the pixel vary from 200 to 600 nm. A dip at  $\approx 470$  nm that changes with the periods can be observed, meaning that the reflection of short wavelength band is suppressed in some content, further resulting in the different colors as the inset shows. And the middle panel is the reflective curve for the pixels with fixed height (300 nm) and period (400 nm) but changed width. The average intensity of the reflection beam is decreased when the edge length changed from 100 to 300 nm, indicating the brightness of the color can be tuned efficiently, which can be found in the inset. As the right panel of **Figure 5b** shows, although the edge length and the period are fixed, both the resonant wavelength and the modulation depth of the reflection have an obvious shift with the increasing height, meaning that the height of the nanopillars gives an effective tunable degree to the structural color. According to **Figure 5b**, thanks to the tunable height of the pixels, the reflective spectra of the light become more controllable. The resonance wavelength, bandwidth, and modulation depth of the spectra can

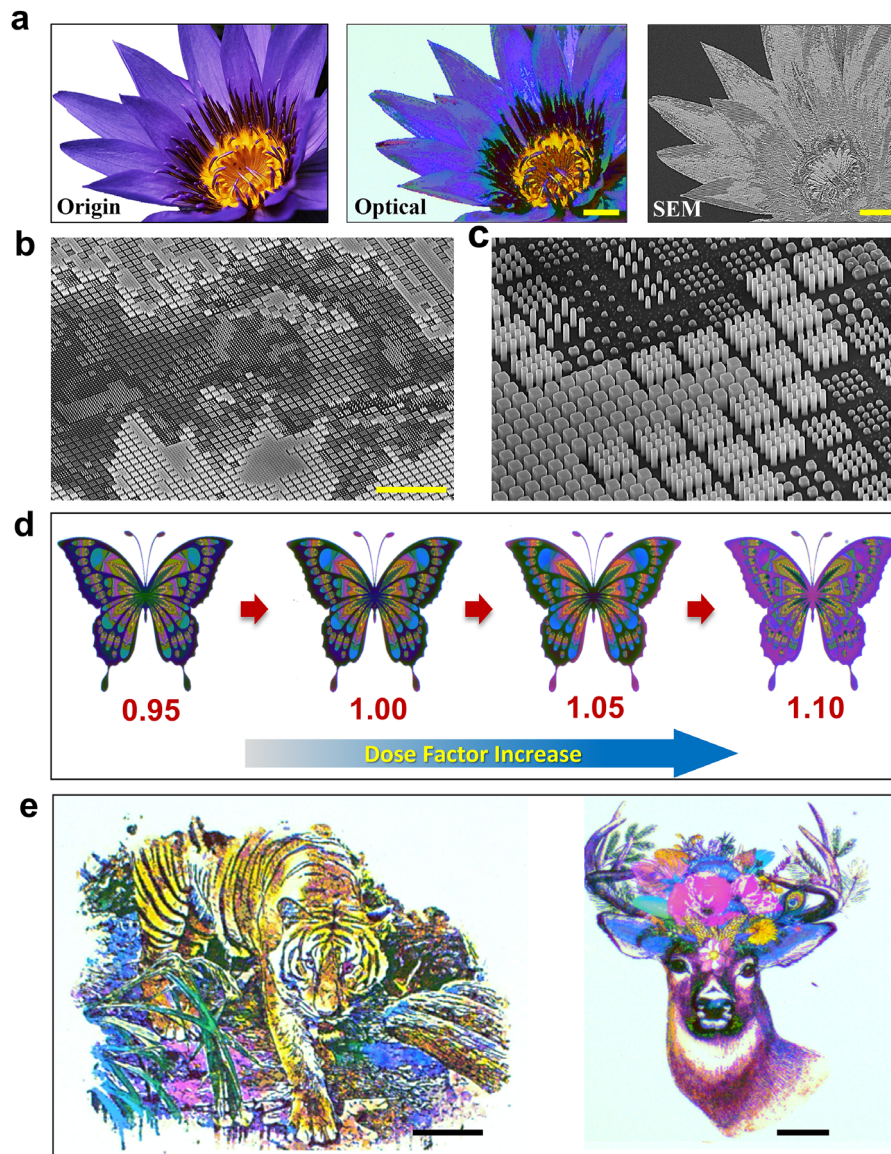


**Figure 6.** Color reproduction ability of the structural color metasurface after introducing height regulation into X–Y plane. a) A comparison between original picture and as-fabricated structural color metasurface including its optical micrograph and a large area SEM image; b) Large area and c) its details of the micro-pixels with real three-dimensions structure regulation in X–Y–Z directions; d) Imaging effect control of colorful butterfly patterns changed with exposure dose factor from 0.95 to 1.1 along with arrow direction; e) Tiger and deer-head images are vividly displayed by as-fabricated structural color metasurface with height regulation in X–Y plane. Scale bar: (a) 100  $\mu\text{m}$ ; (b) 15  $\mu\text{m}$ ; (c) 2  $\mu\text{m}$ ; f) 100  $\mu\text{m}$ .

be independently regulated, resulting in the complete control of the whole HSB space.

Thanks to the grayscale assembly method that can independently tune the height of the meta-pixel, the HSB of the color can be tuned in a more complete and wider range compared to the planer structures. Thus, a series of metasurface consisting of pixel arrays with different height, period, and linewidth are fabricated to construct a library between the feature sizes of pixel and HSB of light. Figure 5c depicts a 3D color map, in which the three axes refer to the height, period, and linewidth, respectively. Further, the structural colors with different hue, saturation, and brightness that rely on the feature sizes of the pixels can be intuitively observed. A color distribution based on HSB

space has been built up and demonstrated in Figure 5d, in which each point means a specific color that relates to a set of feature sizes in the library. Most of the color space is already occupied by realized structural colors due to the outstanding light controllability of height-varying metasurfaces, meaning that the height controllability of structures brought a more abundant color space compared with the structural color based on metasurface of equal height, which are mostly used to tune the CIE color space with only two controllable degrees.<sup>[31]</sup>

According to the design of height-tunable structural color metasurface and its superior color rendering ability above, some typical images of structural color metasurface are shown in **Figure 6**. Based on the color library, the HSB value of each pixel on the

image is extracted and compared for the color optimization, and a layout can be built up by patterns with different widths, periods, and doses (height). In Figure 6a, an original colorful photo of the flower (the left) is perfectly presented by high-resolution structural color coming from the height-varying metasurface (the middle), which is a good restoration of the vivid original color. A top-view SEM image of this structural color metasurface (the right) shows the profile of the flower, in which different grayscale corresponding to the areas with different colors indicates the heights of the nanopillars are effectively controlled in this metasurface. This height-controlled structural color metasurface contains  $500 \times 342$  pixels in a size of  $1.5 \times 1.5 \mu\text{m}$ , meaning that the image have a resolution of  $> 2.86 \times 10^8$  dpi. Figure 6b,c give enlarged details in the center area of structural color metasurface, from which we can see that the pixels in the metasurface have been reliably fabricated, the pixels in the metasurface have distinct edges, guaranteeing the high performance of the structural color metasurface. Noticeably, the nanopillars in a pixel show uniformity configurations in all axes, while the widths, heights, and the periods can be well distinguished for the adjacent pixels. The heights of the unit cells, which is related to the e-beam dose, become a new controllable degree in controlling the structural color, thus the structural color can be tuned by the dose factor of EBL. Figure 6d shows a series of pictures of a butterfly, in which with the original e-beam dose multiplied by a dose factor changing from 0.95 to 1.10, the color of the butterfly can be further changed by the tunable heights of the metasurface even if the picture layout is confirmed. Thanks to the color controllability of the height varying metasurface, diverse images with vivid color can be painted by microscale pixels.

Figure 6e shows the fabricated structural color metasurfaces of a tiger and a deer-head with abundant color in millimeter scale, respectively, showing that the universality of GANF method in the fabrication of colorful displays. The height controllability within a single array enables the complete regulation of the HSB of the structural color, which leads to a rich color library, and resulting in a vivid color reproduction ability consistent with the original picture. This multi-dimensional structure regulation driven by height regulation not only brings great vitality to high-resolution structural color imaging, but also provides more regulation possibilities of light field for other metasurface devices.

### 3. Conclusion

We developed a grayscale assembling nanofabrication method to construct height-individually-tunable nanostructure arrays, which further achieves arbitrary structure control in Z direction and X–Y direction simultaneously. Following this nanofabrication strategy, the real nanoscale multi-dimensional structure regulation can be realized, including X–Y–Z three directions with plane rotation angle ( $\theta$ ), which will provide more possibilities for complex configurations and arrangements of 3D nanostructures and its arrays. A wide range of controllability and a large gray scale in this process enable the powerful ability in height regulation, such as up to 10:1 in aspect ratio and 256 grayscale levels in principle. Tunable height with flexible controllability is introduced to the grayscale images and structural color imaging, giving a fresh regulated approach for high quality nanoscale imaging. Ultra-high-resolution ( $6.4 \times 10^{10}$  dpi) grayscale display

is first obtained, where the height of one single nanopillar can be used to tune the gray level of grayscale images. Moreover, microscale pixels ( $1.5 \mu\text{m}$ ) based on tunable heights demonstrate a more complete controllability of the HSB color space, which enables the ultra-realistic structural-color imaging. The newly developed grayscale nanofabrication method by height-varying nanostructure greatly improves high-resolution grayscale imaging and structural color devices, but also opens a new horizon to design and achieve diversified optical metasurface and optoelectronic components with higher performance and smaller footprint.

### 4. Experimental Section

**Sample Fabrication:** The fabricated process started from the spin coating of the water soluble film (AR-PC 5090.02, purchased from German-Tech) with 40 nm in thickness on a  $2 \text{ cm} \times 2 \text{ cm}$  Si substrate, followed by the spin coating of PMMA (950K, A7) resist of 800 nm, where the rotate speed was set to 2000 rpm. Successively, the patterns with different shapes were exposed under varying doses by EBL system (Raith EBPG 5200), the high tension and the beam current of the EBL were fixed at 100 kV and 5 nA, while the irradiation dose can be selected from 500 to  $1300 \mu\text{C cm}^{-2}$  to achieve height varying nanotemplate. And then the exposed resist was removed by immersing the sample in MIBK/IPA (1:3) solution for 1 min. After developing, the reflow process could be conducted alternatively, and then the achieved nanoholes with different depths were filled by  $\text{TiO}_2$  film via a home-built ALD system. In the above process,  $\text{H}_2\text{O}$  was used as the O source, and Tetrakis (dimethylamino) titanium (TDMAT) precursor was used as the Ti source, which was heated to  $75^\circ\text{C}$  to achieve the required vapor pressure. The ALD system is under continuous 20 sccm flow of  $\text{N}_2$  carrier gas and maintained at  $105^\circ\text{C}$ , the pulse time for both sources were 0.15 s while the purge time was 25 s. throughout the process. Afterward, the substrate was immersed in water to dissolve the water-soluble film, resulting in a substrate-free film composed of PMMA and  $\text{TiO}_2$ . Then the substrate-free film was overturned and transferred to the target substrate, which could be chosen as silicon, quartz, polydimethylsiloxane (PDMS), or Al film. Finally, the height-varying structures could be obtained after removing the residual resist ( $\text{O}_2$  flow of 50 sccm, pressure of 100 mTorr, RF power of 100 W) and underneath  $\text{TiO}_2$  film ( $\text{CHF}_3$  flow of 25 sccm, Ar flow of 5 sccm, RF power of 30 W, ICP power of 500 W) by a dry etching process in an ICP-RIE system (Plasmalab System 100 ICP180, Oxford).

**Configuration Characterization:** The height-varying nanostructures and the grayscale micro-images were loaded into the SEM (Hitachi, Regulus 8230) chamber, then the samples were irradiated by the e-beam of 15 keV energy. The feature size of the structures can be measured by the built-in program of the controlling software. And to obtain the best imaging quality, a 10 nm Cr was deposited to the samples on dielectric substrate.

**Optical Setup:** The reflection spectra of the structural color metasurfaces were collected by a microscopic spectrometer, where the light source was a halogen light source (HL2000), whose operating wavelength ranged from 360 to 2500 nm, and a spectrometer (PG2000) was used to collect the reflection signals of the metasurface with different colors. And the colorful micrography of the metasurface was collected by a CCD camera after a  $10\times$  objective lens.

### Supporting Information

Supporting Information is available from the Wiley Online Library or from the author.

### Acknowledgements

The authors acknowledge the financial support received from the National Natural Science Foundation of China (grant nos. 12204527, 12074420,

U21A20140, and 61905274), the Beijing Municipal Science & Technology Commission, Administrative Commission of Zhongguancun Science Park (no. Z211100004821009), the Chinese Academy of Sciences through the Project for Young Scientists in Basic Research (YSBR-021), and the Key Research Program of Frontier Science, Chinese Academy of Sciences (grant no. QYZD-J-SSW-SLH042). This work was also supported by the Synergic Extreme Condition User Facility (SECUF).

## Conflict of Interest

The authors declare no conflict of interest.

## Data Availability Statement

Research data are not shared.

## Keywords

grayscale e-beam lithography, grayscale images, height varying nanostructures, structural color, ultra-high-resolution painting

Received: January 29, 2023

Revised: March 10, 2023

Published online:

- [1] a) Z. Ren, Y. Chang, Y. Ma, K. Shih, B. Dong, C. Lee, *Adv. Opt. Mater.* **2019**, *8*, 1900653; b) G. R. Bhatt, B. Zhao, S. Roberts, I. Datta, A. Mohanty, T. Lin, J. M. Hartmann, R. St-Gelais, S. Fan, M. Lipson, *Nat. Commun.* **2020**, *11*, 2545.
- [2] a) D. Palaferri, Y. Todorov, A. Bigioli, A. Mottaghizadeh, D. Gacemi, A. Calabrese, A. Vasanelli, L. Li, A. G. Davies, E. H. Linfield, F. Kapsalidis, M. Beck, J. Faist, C. Sirtori, *Nature* **2018**, *556*, 85; b) B. C. Zhang, Y. H. Shi, J. Mao, S. Y. Huang, Z. B. Shao, C. J. Zheng, J. S. Jie, X. H. Zhang, *Adv. Mater.* **2021**, *33*, 2008171.
- [3] a) X. Yin, J. Jin, M. Soljacic, C. Peng, B. Zhen, *Nature* **2020**, *580*, 467; b) Y. Y. Xie, P. N. Ni, Q. H. Wang, Q. Kan, G. Briere, P. P. Chen, Z. Z. Zhao, A. Delga, H. R. Ren, H. D. Chen, C. Xu, P. Genevet, *Nat. Nanotechnol.* **2020**, *15*, 125.
- [4] a) X. Chen, H. R. Park, M. Pelton, X. Piao, N. C. Lindquist, H. Im, Y. J. Kim, J. S. Ahn, K. J. Ahn, N. Park, D. S. Kim, S. H. Oh, *Nat. Commun.* **2013**, *4*, 2361; b) Y. Chen, Q. Xiang, Z. Li, Y. Wang, Y. Meng, H. Duan, *Nano Lett.* **2016**, *16*, 3253.
- [5] a) S. S. Masango, R. A. Hackler, N. Large, A. I. Henry, M. O. McAnally, G. C. Schatz, P. C. Stair, R. P. Van Duyne, *Nano Lett.* **2016**, *16*, 4251; b) Y. Yang, R. Pan, S. Tian, C. Gu, J. Li, *Micromachines* **2020**, *11*, 1109.
- [6] a) H. Li, C. Xie, *Micromachines* **2020**, *11*, 378; b) T. Lin, S. Ramadurgam, C. S. Liao, Y. Zi, C. Yang, *Nano Lett.* **2015**, *15*, 4993.
- [7] a) A. A. Femius Koenderink, A. Polman, *Science* **2015**, *348*, 516; b) V. A. Fedotov, P. L. Mladonov, S. L. Prosvirnin, A. V. Rogacheva, Y. Chen, N. I. Zheludev, *Phys. Rev. Lett.* **2006**, *97*, 167401; c) K. A. Arpin, A. Mihi, H. T. Johnson, A. J. Baca, J. A. Rogers, J. A. Lewis, P. V. Braun, *Adv. Mater.* **2010**, *22*, 1084.
- [8] Y. Bao, J. Ni, C. W. Qiu, *Adv. Mater.* **2020**, *32*, 1905659.
- [9] J. Zhou, T. Koschny, M. Kafesaki, E. N. Economou, J. B. Pendry, C. M. Soukoulis, *Phys. Rev. Lett.* **2005**, *95*, 223902.
- [10] a) A. H. Dorrah, F. Capasso, *Science* **2022**, *376*, eabi6860; b) N. Yu, F. Capasso, *Nat. Mater.* **2014**, *13*, 139; c) F. Wang, G. Geng, X. Wang, J. Li, Y. Bai, J. Li, Y. Wen, B. Li, J. Sun, J. Zhou, *Adv. Opt. Mater.* **2021**, *10*, 2101842.
- [11] a) H. Wang, Q. Ruan, H. Wang, S. D. Rezaei, K. T. P. Lim, H. Liu, W. Zhang, J. Trisno, J. Y. E. Chan, J. K. W. Yang, *Nano Lett.* **2021**, *21*, 4721; b) Z. Liu, J. Li, Z. Liu, W. Li, J. Li, C. Gu, Z. Y. Li, *Sci. Rep.* **2017**, *7*, 8010.
- [12] S. Li, X. Li, G. Wang, S. Liu, L. Zhang, C. Zeng, L. Wang, Q. Sun, W. Zhao, W. Zhang, *Adv. Opt. Mater.* **2018**, *7*, 1801365.
- [13] R. Zhao, X. Xiao, G. Geng, X. Li, J. Li, X. Li, Y. Wang, L. Huang, *Adv. Funct. Mater.* **2021**, *31*, 2100406.
- [14] G. Kim, Y. Kim, J. Yun, S. W. Moon, S. Kim, J. Kim, J. Park, T. Badloe, I. Kim, J. Rho, *Nat. Commun.* **2022**, *13*, 5920.
- [15] W. Yang, S. Xiao, Q. Song, Y. Liu, Y. Wu, S. Wang, J. Yu, J. Han, D. P. Tsai, *Nat. Commun.* **2020**, *11*, 1864.
- [16] a) W. L. Hsu, P. C. Wu, J. W. Chen, T. Y. Chen, B. H. Cheng, W. T. Chen, Y. W. Huang, C. Y. Liao, G. Sun, D. P. Tsai, *Sci. Rep.* **2015**, *5*, 11226; b) J. Chen, C. Zhang, Q. Cheng, presented at *2019 IEEE MTT-S International Wireless Symposium (IWS)*, 19–22 May 2019, **2019**; c) S. Wang, X. Sun, D. Chen, S. Wang, Y. Qi, F. Wu, *Opt. Commun.* **2020**, *460*, 125129.
- [17] a) S. M. Sajadi, P. S. Owuor, S. Schara, C. F. Woellner, V. Rodrigues, R. Vajtai, J. Lou, D. S. Galvao, C. S. Tiwary, P. M. Ajayan, *Adv. Mater.* **2018**, *30*, 1704820; b) Y. Hu, Z. Lao, B. P. Cumming, D. Wu, J. Li, H. Liang, J. Chu, W. Huang, M. Gu, *Proc. Natl. Acad. Sci. U. S. A.* **2015**, *112*, 6876.
- [18] a) H. Wang, H. Wang, Q. Ruan, Y. S. Tan, C. W. Qiu, J. K. W. Yang, *ACS Nano* **2021**, *15*, 10185; b) X. Xiong, X. Wang, Z. Wang, Y. Gao, R. Peng, M. Wang, *Opt. Lett.* **2021**, *46*, 1193.
- [19] M. Esposito, V. Tasco, M. Cuscunà, F. Todisco, A. Benedetti, I. Tarantini, M. D. Giorgi, D. Sanvitto, A. Passaseo, *ACS Photonics* **2014**, *2*, 105.
- [20] M. Christophersen, B. F. Philips, *Appl. Phys. Lett.* **2008**, *92*, 194102.
- [21] C. Wan, C. Dai, J. Zhang, S. Wan, Z. Li, G. Zheng, X. Zhang, Z. Li, *Small* **2021**, *17*, e2100561.
- [22] a) C. Dai, C. Wan, Z. Li, Z. Wang, R. Yang, G. Zheng, Z. Li, *Adv. Opt. Mater.* **2021**, *9*, 2100950; b) C. Dai, Z. Wang, Y. Shi, Z. Li, Z. Li, *Nano Lett.* **2022**, *22*, 9990.
- [23] C. Dai, Z. Li, Z. Li, Y. Shi, Z. Wang, S. Wan, J. Tang, Y. Zeng, Z. Li, *Adv. Funct. Mater.* **2022**, *33*, 2212053.
- [24] G. Geng, W. Zhu, R. Pan, Z. Zhang, C. Gu, J. Li, *Nano Today* **2021**, *38*, 101145.
- [25] a) C. Xu, S. Zhang, J. Shao, Y. Chen, *Microelectron. Eng.* **2018**, *196*, 1; b) A. Schleunitz, H. Schiff, *J. Micromech. Microeng.* **2010**, *20*, 095002.
- [26] J. K. W. Yang, H. Duan, J. B. K. Law, H. Y. Low, B. Cord, *J. Vac. Sci. Technol., B: Nanotechnol. Microelectron.: Mater., Process., Meas., Phenom.* **2011**, *29*, 06F313.
- [27] a) F. Yue, C. Zhang, X. F. Zang, D. Wen, B. D. Gerardot, S. Zhang, X. Chen, *Light: Sci. Appl.* **2018**, *7*, 17129; b) J. Li, Y. Wang, C. Chen, R. Fu, Z. Zhou, Z. Li, G. Zheng, S. Yu, C. W. Qiu, S. Zhang, *Adv. Mater.* **2021**, *33*, 2007507.
- [28] M. Vatankehah-Varnosfaderani, A. N. Keith, Y. Cong, H. Liang, M. Rosenthal, M. Sztucki, C. Clair, S. Magonov, D. A. Ivanov, A. V. Dobrynin, S. S. Sheiko, *Science* **2018**, *359*, 1509.
- [29] J. Xue, Z. K. Zhou, Z. Wei, R. Su, J. Lai, J. Li, C. Li, T. Zhang, X. H. Wang, *Nat. Commun.* **2015**, *6*, 8906.
- [30] M. Song, L. Feng, P. Huo, M. Liu, C. Huang, F. Yan, Y. Q. Lu, T. Xu, *Nat. Nanotechnol.* **2023**, *18*, 71.
- [31] a) X. Liu, Z. Huang, J. Zang, *Nano Lett.* **2020**, *20*, 8739; b) W. Yue, S. Gao, S. S. Lee, E. S. Kim, D. Y. Choi, *Laser Photonics Rev.* **2017**, *11*, 1600285.